Science of the Total Environment 781 (2021) 146710

Contents lists available at ScienceDirect

Science of the Total Environment

journal homepage: www.elsevier.com/locate/scitotenv

Assessment of seawater intrusion under different pumping scenarios in Moghra aquifer, Egypt

Samar Mohamed Gomaa [a,*], Taher Mohammed Hassan [a], Esam Helal [b]

[a] Research Institute for Groundwater, National Water Research Center, Cairo, Egypt
[b] Civil Engineering Department, Faculty of Engineering, Menoufia University, Egypt

HIGHLIGHTS

- In this research, a 3-D numerical model for flow and solute transport has been built using the SEAWAT module.
- The model shows the quantitative and qualitative changes in the aquifer under different pumping conditions considering SWI.
- The procedure followed for SWI simulation and calibration process depends on two different approaches.
- Mass balance calculations were shown to describe how the conceptual model works.
- Sensitivity analysis has been set up for the model parameters to describe the uncertainty degree.

GRAPHICAL ABSTRACT

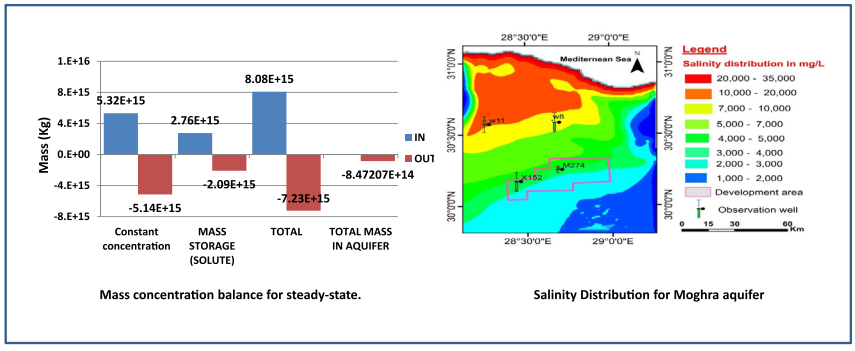

Mass concentration balance for steady-state.

Salinity Distribution for Moghra aquifer

ARTICLE INFO

Article history:
Received 22 January 2021
Received in revised form 17 March 2021
Accepted 19 March 2021
Available online 25 March 2021

Editor: Damia Barcelo

Keywords:
Groundwater
Moghra aquifer
Numerical modeling
Seawater intrusion
Mass balance
Sensitivity analysis

ABSTRACT

The Moghra aquifer has shown promise in land reclamation projects conducted in the Western Desert of Egypt. Although this aquifer has hundreds of pumping wells in new urban communities built to meet the needs of the increased population, the system is threatened by the phenomenon of seawater intrusion (SWI). The present study evaluates the degree to which these pumping wells will attract seawater to the aquifer system in the Western Desert region under different pumping conditions. Using the SEAWAT module of Groundwater Modeling System (GMS) software, a three-dimensional (3D) finite-difference model is built to simulate the flow and salinity distribution in the Moghra aquifer considering the geological and hydrogeological characteristics of the aquifer system. The procedure used to solve the mathematical model relied on merging two different approaches. The first approach described the dividing lines of the transition zone due to the SWI. The second approach was applied to conduct the perfect calibration process for the aquifer system. The results show that the flow and quality of the groundwater aquifer are affected by pumping. The water level and salinity are predicted under different pumping rates, a fivefold increase in the pumping rate results that the salinity increased between 4% and 26.8% according to the well location. Moreover, the drawdown values reached 162 m, which is about 46.3% of the saturated thickness.

1. Introduction

Groundwater has become the savior resource for freshwater in many countries globally, particularly in arid and semi-arid regions

* Corresponding author.
E-mail addresses: samar.mohamed2281@gmail.com, samar_gomaa@nwrc.gov.eg (S.M. Gomaa), drtahermh@yahoo.com (T.M. Hassan), esameman@yahoo.com, Esamhelal@sh-eng.menofia.edu.eg (E. Helal).

https://doi.org/10.1016/j.scitotenv.2021.146710
0048-9697/

such as Egypt (Negm, 2019). Substantial increases in population and surface water limitations have motivated the government to search for alternate water resources, such as groundwater and water from seawater desalinization. The Egyptian government has announced plans to expand development in the Western Desert to reduce the pressure on surface water resources, especially after the Grand Ethiopian Renaissance Dam construction, which reduced Egypt's quota from the Nile River (Abdelhaleem and Helal, 2015). The residents of Moghra, a newly developed area, depend on the Moghra aquifer to cater to their water demands. Since this body is considered an essential aquifer in the northern region of the Western Desert, it should be well managed to ensure its adequacy for sustained development. Groundwater contamination can be caused by many factors (Allam et al., 2019; Mansour et al., 2018), the most common of which is seawater intrusion (SWI). This factor is a natural phenomenon by which the salt water of the sea can replace the freshwater of the aquifer (Badaruddin et al., 2017). Badaruddin and Morgan (2017) categorize the SWI into active and passive. It depends on the direction of the freshwater direction if toward the sea or the land.

Many studies on SWI based on monitoring systems and modeling have been conducted. The simulation of SWI is considered to be a complex process, and the results differ among aquifers according to their natures (Sefelnasr and Sherif, 2014). Pool et al. (2014, 2015) showed the difference of homogeneity and heterogeneity in the hydraulic conductivity on SWI and solute spreading. Modeling is a useful tool for defining an aquifer, simulating its phase, and predicting its behavior under various conditions (Sobeih et al., 2017). Two approaches can be used for simulating SWI. The first is the sharp interface approach, which depends on the Ghyben–Herzberg relation assuming that the fresh water and saltwater are not miscible and are separated by a sharp interface. The second is the transition zone approach, which assumes a diffusion interface between the two water types (Sakr, 1992; Sherif et al., 2014). Sakr et al. (2004) used an analytical model using the sharp interface approach to determine the thickness of the freshwater that occupies the Nile Delta Aquifer. Guo and Langevin (2002) used the FEFLOW computer program to develop a groundwater flow and solute transport numerical model to test the effects of pumping on SWI. In their study, many scenarios were applied, which considered pumping rate, number of wells, and well location to determine the optimal case with the least intrusion. Sherif et al. (2014) used a numerical model using the FEFLOW software to simulate a coastal aquifer under various pumping scenarios. The model showed that reducing the pumping rate could mitigate SWI, whereas increasing the pumping rate could accelerate SWI toward the freshwater zone and reduce the volume of fresh water in the aquifer. Nofal et al. (2015) used the SEAWAT software program to build a detailed conceptual regional model that illustrated the effect of SWI on the Nile Delta aquifer. The model showed that SWI mainly occurred in shallow and medium depths. Abu-Bakr et al. (2016) used numerical modeling to investigate the effect of groundwater abstraction from a coastal aquifer. The model predicted the salinity and water levels under various scenarios and showed a direct relationship between the wells arrangement and the enhancement of groundwater quality. Chang et al. (2018) simulated the SWI for coastal aquifers using a 2D SEAWAT model to predict the interface between the brine and freshwater for specific forecasting as well as the changes in water level caused by pumping. Farooq (2020) presented an explanation for the SWI phenomenon and its controlling factors and discussed several methods for mitigating its effect. Kazakis et al. (2018) used a six parameters-dependent method for modifying the standard method for the GALDIT-F method which explains the seawater intrusion assessment in a coastal aquifer. Many other studies were discussed in SWI Meetings as a review for the groundwater quality influenced by the SWI phenomenon (Sarker et al., 2018; Stein et al., n.d.; Langevin et al., 2016; Polemio and Zuffianò, 2013; Oude Essink and Boekelman, 1998; Verkaik et al., 2018). Abdel Mogith et al. (2013) investigated the Moghra aquifer to determine the best physical, chemical, and hydrological configurations. The salinity of the aquifer in the study area was 5000–10,000 mg/L; this wide range is attributed to changes in the depositional environment of the Moghra Formation from continental to marine.

The previous studies help to explain the mechanism of SWI simulation in aquifers and the geological and hydrogeological settings of the Moghra aquifer. However, very little has been reported on the effect of SWI on the Moghra aquifer. Also, there are not many researches to discuss the active SWI studies, which is the same situation in Moghra aquifer case. Therefore, the objective of the present study is to assess the impact of groundwater extraction from the Moghra aquifer considering the SWI phenomenon under many different scenarios.

2. Study area

2.1. Site description

The study area is located in the northern part of the Western Desert in Egypt. It extends between the geographical coordinates of 28°10′, 29°20′ E longitude and 29°50′, 31°10′ N latitude. The development area for the pumping wells is about 60 km from the coast; looking south (Fig. 1). The study area is located in the northwestern coastal zone of the subtropical Mediterranean climate, which includes mild and wet winters and hot and dry summers. Matrouh receives average annual precipitation of 155 mm in the winter season (Yousif and Bubenzer, 2012).

2.2. Hydrogeology

The groundwater in the study area is stored mainly in four aquifers of Tertiary and Quaternary ages (Morad et al., 2014).

2.2.1. The northern aquifer system

The northern region of the study area is a complex system consisting of three aquifers connected by a leaky connection that are directly affected by SWI (Sayed, 2018). Their characteristics, listed below, are a secondary concern in this research owing to their rare occurrence in the study area.

a. Unconsolidated Coastal Dune Aquifer (Holocene):

This aquifer consists of white carbonate sands. The groundwater exists in unconfined conditions and is recharged by annual rainfall. It exists in a long, thin strip oriented parallel to the Mediterranean Sea coast in the easternmost part of the area and has an area of about 2000 km^2 or 13% of the total area; its thickness reaches 30 m The northern boundary of this aquifer merges gradually to the sea (Yousif and Bubenzer, 2013).

b. Pliocene Limestone Aquifer:

This Tertiary aquifer underlies the previous sand aquifer and overlies the Upper Miocene aquifer with a thickness reaching 38 m. It is composed of hard limestone and is recharged by direct rainfall and SWI. The groundwater exists in unconfined to confined conditions. These limestone deposits cover an area of about 4480 km^2 or 30% of the total area (Sayed, 2018).

c. Upper Miocene Aquifer (Marmarica Aquifer):

This Miocene aquifer consists of limestone with thicknesses of 50–250 m and has not penetrated by any wells in the study area domain. It lies to the north of the area with a wide distribution of about 6500 km^2 or 43% of the total area. The water in the aquifer exists in free water conditions (unconfined). The aquifer is recharged by rainfall and downward leakage from the overlying Pleistocene aquifer (Yousif and Bubenzer, 2013). The groundwater found inside the limestone ridges originates directly from infiltration and percolation of annual

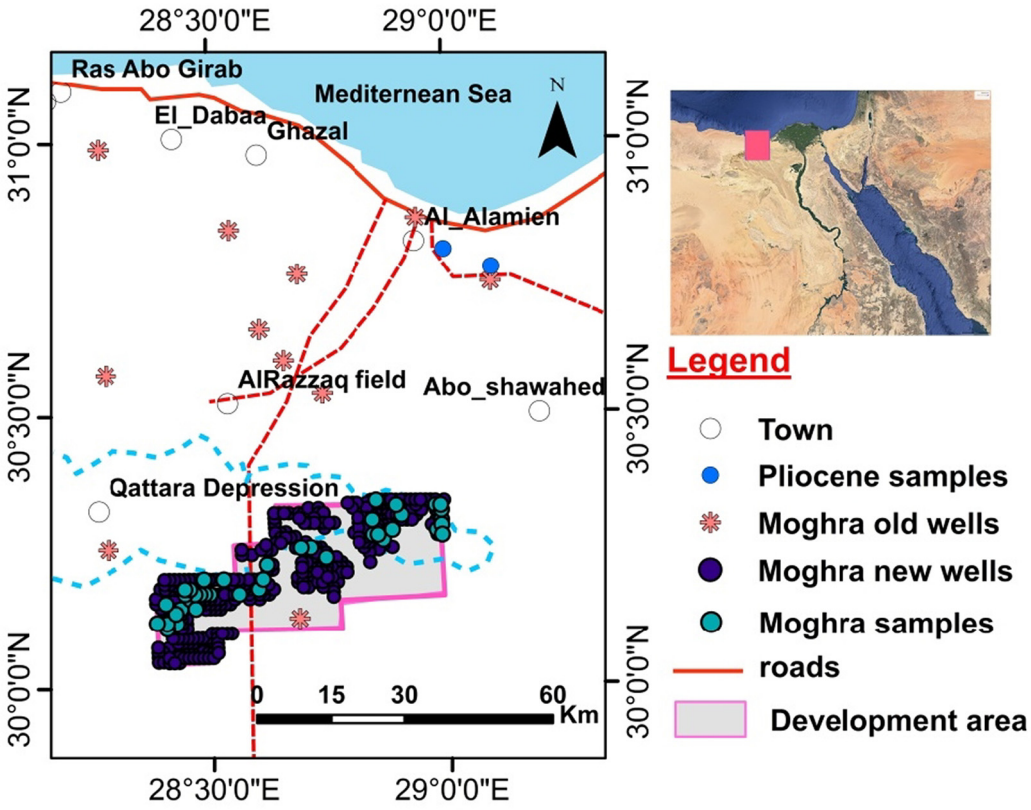

Fig. 1. Location map of the study area and samples sites.

rainfall on the ridges or rainwater falling on the tableland located to the south (Abdel Mogith et al., 2013).

All these aquifers tend to disappear in the southern part of the study area near the development area, where the Moghra aquifer appears at the surface.

2.2.2. Moghra aquifer (Lower Miocene Aquifer)

This Miocene aquifer consists of sandstone with intercalations of shale and coarse sand lenses (Abdallah, 1966). It represents the main aquifer system of the study area with thicknesses of 0–500 m and is underlain by Oligocene Dabaa shale (Abdel Mogith et al., 2013). It covers a wide space from the north to the Western Desert and is bordered by the Nile Delta in the east, the Mediterranean coast in the north, and the Bahariya–Abu Roash uplift in the south with a 50,000 km^2 area (Sayed, 2018). The entire area study is covered by the Moghra aquifer, although it expands past the area domain. The aquifer acts as an unconfined aquifer in the southern half of the area near the development area, but it is under confined conditions in the northern part (RIGW, 2018; Fig. 2).

3. Methodology

3.1. Data analysis and sampling

In this research, about 450 wells drilled in 2018 by the Ministry of Water Resources and Irrigation in only two aquifers from the previously stated aquifers were analyzed (Table 1). For the collected data, groundwater levels in the Moghra aquifer were between −10 m and −60 m, and the main groundwater flux is directed from the northeast to southwest. About 96 samples were taken from Moghra aquifer's screens to measure the salinity of the aquifer water. Their salinity is 1200–9800 mg/L. On the other hand, historical data of only 20 wells distributed in different locations over the whole area through the aquifer shows that the total dissolved solids ranged from 3300 to 10,100 mg/L. This data helped to have a salinity concentration distribution for Moghra aquifer. On the contrary, the water levels of the Pliocene limestone aquifer range between 6 m and 24 m. The flow direction is from the south toward the sea in the north. It is worth noting that the majority of the Pliocene aquifer samples are seawater ones of 42,000 mg/L. They were too shallow and taken from 20 to 40 m depth; only one sample has TDS of 8813 mg/L. It was noticed that a wide range of salinity variations was detected in the taken samples from the drilled wells in the aquifer system, which means that the groundwater in the aquifer system is brackish according to the classification of Davis and De Wiest (1967), as shown in Table 2. These data helped in simulating the aquifer system to obtain the initial visualization of its water quality. Fig. 1 illustrates the distribution of the case study wells and samples' locations, as well as that of the aquifers they penetrate.

3.2. Model setup

Moghra aquifer management concerning the phenomenon of SWI is considered to be a complex process. Aside from the difficulty of simulating the process itself, the aquifer in the study area had not been pumped. Moghra salinization situation is critical as the groundwater flow direction is the same as the seawater, which is called active SWI, so there is a big chance for intrusion under pumping conditions. Accordingly, a numerical model was built for case simulation. Using the SEAWAT module of Groundwater Modeling System (GMS) software, a 3D model for groundwater flow and salt transport was created to simulate the groundwater flow and saltwater intrusion for the aquifer system considering all the available hydrogeological characteristics, calibrate the system and predict the aquifer behavior under several pumping conditions. The SEAWAT module combines two modules. The first module, MODFLOW, is used to solve the groundwater flow and movement direction problem, and the second one, MT3DMS, is used for solute transport problems (Guo and Bennett, 1998).

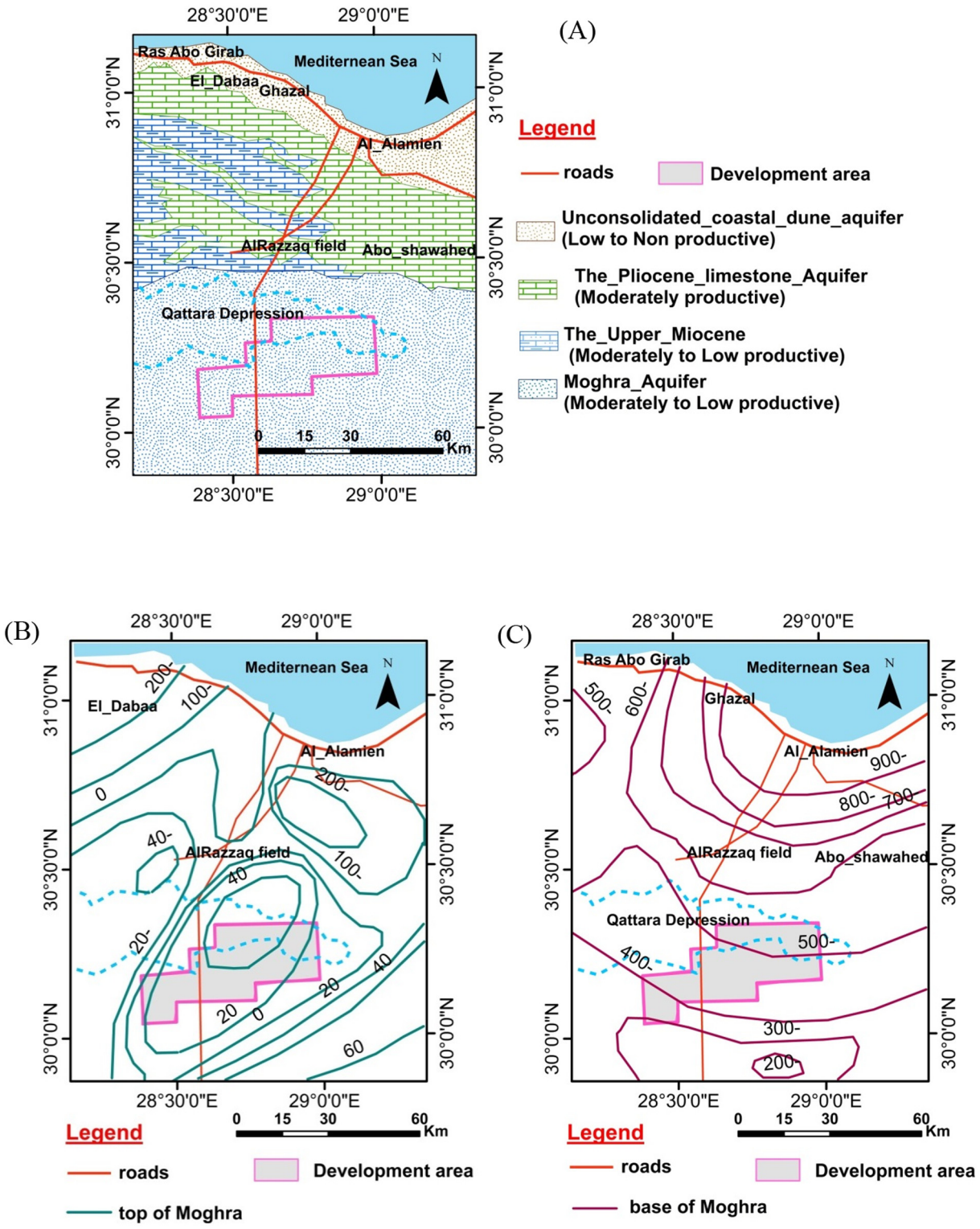

Fig. 2. (A) Aquifers of the study area, (B) top of the Mogha aquifer and (C) base of the Moghra aquifer after (Ezzat, 1984; RIGW, 2006).

Table 1
Wells located in the case study domain data (RIGW, 2018; Ezzat, 1984).

		Well no.	Penetrated aquifer	Total depth (m)	D.T.W. (m)	Water level (m)	TDS (mg/L)	Q (m^3/h)
450 wells	New samples	445	Mogha	90:200	(30:90)	(−10:−60)	1200:9800	Not yet pumped
		5	Pliocene	15:110	(2.1:18.8)	(6:24)	8813:42,000	
20 wells	Literature	20	Mogha	275:985	(−1: 297)	(−26:−48.7)	3300:10,100	8:108

Table 2
Groundwater type classification according to Davis and De Wiest (1967).

Water type	Concentrations in mg/L
Fresh water	0–1000
Brackish water	1000–10,000
Saline water	10,000–100,000
Brines	>100,000

3.2.1. Governing equation

The governing equation of the groundwater flow used for variable density is

$$\frac{\partial}{\partial x}\left(\rho K_{fx}\left[\frac{\partial h_f}{\partial x}+\left(\frac{\rho-\rho_f}{\rho_f}\right)\frac{\partial Z}{\partial x}\right]\right)+\frac{\partial}{\partial y}\left(\rho K_{fy}\left[\frac{\partial h_f}{\partial y}+\left(\frac{\rho-\rho_f}{\rho_f}\right)\frac{\partial Z}{\partial y}\right]\right)+\frac{\partial}{\partial z}\left(\rho K_{fz}\left[\frac{\partial h_f}{\partial z}+\left(\frac{\rho-\rho_f}{\rho_f}\right)\frac{\partial Z}{\partial z}\right]\right)=\rho S_f\frac{\partial h}{\partial t}+\theta\frac{\partial \rho}{\partial C}\frac{\partial C}{\partial t}-\rho_s q_s \quad (1)$$

where h_f is the equivalent freshwater head [m], ρ_f is the density of freshwater [kg/m^3], q_s is the unit volume flow of the source (sink) [1/s], θ is the effective porosity of the porous medium, S_f: is the unit water storage coefficient of equivalent freshwater [1/m], and K_{fs} is the permeability coefficient of the equivalent freshwater [m/s].

The equation of solute transport is

$$\frac{\partial\left(\theta C^k\right)}{\partial t}=\frac{\partial}{\partial x_i}\left(\theta D_{ij}\frac{\partial C^k}{\partial x_i}\right)-\frac{\partial}{\partial x}\left(\theta\, \vartheta i C^k\right)+q_s C^S K+R_n \quad (2)$$

where C^k is the concentration of dissolved salt [mg/L], D_{ij} is the hydrodynamic dispersion coefficient [m^2/s], C_k^s is the salt concentration [mg/L], and R_n is the reaction term of salt (Chang et al., 2018).

3.2.2. Modeled area and aquifer geometry

The simulated area is covered by a grid of 140 rows × 110 columns in the horizontal plane with a cell size of 1000 m × 1000 m. The vertical domain was divided into four layers with different hydrogeological characteristics of approximately 22,380 cells. Fig. 3 shows a 3D view of the model grid.

To avoid unacceptable discretization errors and to reduce the uncertainty in the numerical results, three different mesh types, coarse, medium, and fine were used to test the accuracy of the model simulation. The grid convergence index (GCI) was calculated following that discussed by Roache (1998).

$$GCI_{23}^{fine}=\frac{1.25|E_{23}|}{r_{23}^p-1} \quad (3)$$

$$P=\frac{1}{\ln r_{23}}\,ln\,\frac{\left(r_{23}^p-1\right)e_{12}}{\left(r_{12}^p-1\right)e_{23}} \quad (4)$$

The approximate relative error between the medium and fine grids is E_{23}, where $E_{23}=(\phi_3-\phi_2)/\phi_3$; ϕ_2 and ϕ_3 are the medium and fine grid solutions for the water level in different grid spacings of h2 and h3, respectively; r_{23} = h2/h3; and P is the local order of accuracy (Gumus et al., 2016).

In addition, $e_{12}=\phi_2-\phi_1$ and $e_{23}=\phi_3-\phi_2$, were ϕ_3, ϕ_2, and $\phi 1$ are the water levels in the three different meshes; h3 < h2 < h1; and r_{12} = h1/h2.

The equations give the following calculation parameters:

$r_{12}=1.5$, $r_{23}=2$, $\phi_1=-10$ m, $\phi_2=-10.33$ m, $\phi_3=-10.56$ m, $P=1.69$, and $E_{23}=2.18\%$. Thus, a GCI value of 1.22% is acceptable.

3.2.3. Conceptual model and boundary conditions

The Mediterranean Sea is considered to have a constant head boundary of 0 m and a constant salinity boundary of 35,000 mg/L. The first and second layers represent limestone aquifers composed of Pliocene limestone and Upper Miocene limestone with thicknesses of 38 m and 250

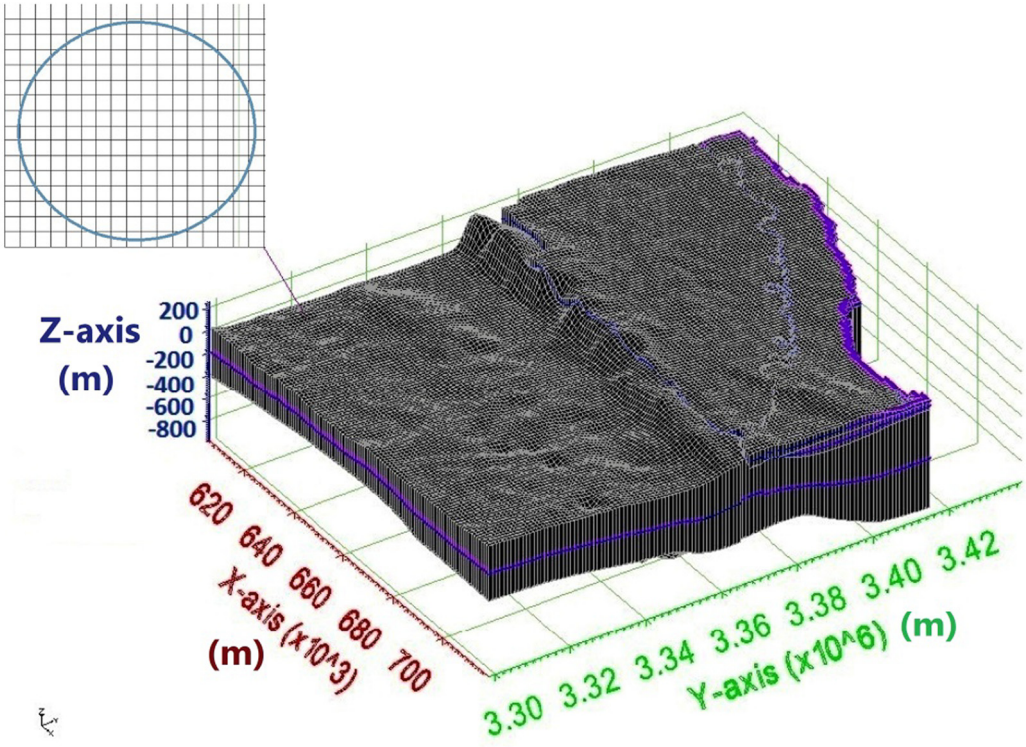

Fig. 3. 3D view of the model grid.

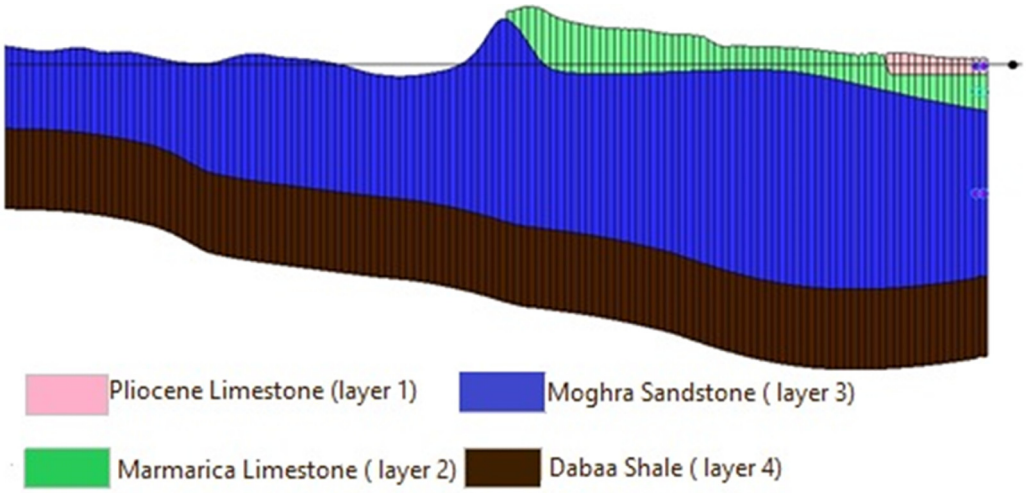

Fig. 4. Conceptual model of the study area.

m respectively. The third layer, which represents the Moghra aquifer, has a thickness of 500 m and reaches 980 m in the northern part of the study area. Moghra is underlain by the fourth impervious layer with low hydraulic conductivity which is considered as an aquitard. Fig. 4 shows the conceptual model for the study area.

3.2.4. Aquifer hydraulic properties

The Moghra hydraulic parameters were obtained from pumping tests analysis conducted on several selected wells using Aquifer Test 2016.1 software. The hydraulic conductivity ranges from 1 m/d to 24 m/d, and the transmissivity values vary at 760–7600 m^2/d. The storativity ranges between 0.1 and 0.001 (Table 3). While the hydraulic conductivity for the Marmarica aquifer and the Pliocene limestone is 0.1–6 m/d and 9.1–39.8 m/d, respectively (Ahmed et al., 2015; Ezzat, 1984).

The created model considered the advection and hydrodynamic dispersion processes for conservative salt transport. The longitudinal dispersivity equaled 1000 m (grid spacing). The transversal horizontal dispersivity and the transversal vertical dispersivity were 0.1 and 0.01 of the longitudinal dispersivity, respectively. The porosity of the sandstone of Moghra and the sandy shales is 26%:50% is and 30%:58%, respectively (Korany, 1975).

4. Results and discussion

The mechanism of the solution was to start with the baseline condition, which describes the current situation without any groundwater extraction because the wells had not been pumped yet. Thus, groundwater extraction during the last 40 years was performed by only 20 wells inside the modeled area domain with very low and non-continuous pumping rates. The baseline condition of the designated model was the year 2018 as the data are available for this year.

To delineate the salinity concentration distribution, two approaches were applied for that particular aspect.

4.1. First approach

Assuming that there is no defined initial concentration distribution for the aquifer system, this approach is suitable for applying in such a case. In this approach, the aquifer starts with completely freshwater mixed with the saline seawater of the Mediterranean Sea, and then it is solved for a long time until a steady-state in the groundwater concentration is attained. This method helps in defining the dividing lines between the saline water, brackish water and fresh water in the aquifer as well as the salinity concentration distribution for the steady-state (Mabrouk et al., 2019).

The model was carried out for 50 simulated stress periods that varied from 1 month to 8000 years. The stress periods start with short time steps in the beginning of the solution then they were gradually set to be longer. These long stress periods facilitate the spread of the salt into the aquifer system: By increasing the stress period length, the groundwater of the aquifer will be salinized rapidly with the coastal saline water. The model was run with the aforementioned stress periods to obtain the salinity concentration distribution for the horizontal and vertical directions (Fig. 5).

Table 3
Calculated hydraulic parameters of several selected Moghra aquifer wells.

Well ID	Aquifer condition	Well depth (m)	Pumping test rate (m^3/h)	DD (m)	T (m^2/d)	η (well efficiency) %	Specific capacity (m^3/h/m)	Well productivity
A139	Unconfined	124	100	3.37	6210	92.77	29.673591	High
X 135	Unconfined	200	110	5.5	3220	92.43	20	High
X 141	Unconfined	198	100	5.5	2910	93	18.18	High
X 186	Unconfined	125	90	3.1	7260	93.44	29.032258	High
X 202	Unconfined	94	98	4	6750	93	24.5	High
X 236	Unconfined	125	102	3.55	7420	93	28.732394	High
X 240	Unconfined	95	89	4.2	6130	92.77	21.190476	High
X 243	Unconfined	98	105	4	7400	92.43	26.25	High
X 252	Unconfined	96	100	3.85	7590	92.77	25.974026	High
X 30	Unconfined	125	95	4.5	5390	92.77	21.111111	High
X 33	Unconfined	125	100	4	6120	92.77	25	High
X 37	Unconfined	125	105	5.2	4470	92.43	20.192308	High
X 7	Unconfined	100	95	3.7	7320	93	25.675676	High
P16prod	Confined	207	35	11.34	759	97	3.08	Moderate

It was noticed that the fresh zone of the modeled area occupied the entire development area, which is not in agreement with the actual conditions. The aquifer itself holds brackish water with salinity at more than 1000 mg/L. Also, the SWI increased with the progress of the simulation time vertically.

4.1.1. Sensitivity analysis

It is only conducted for the steady-state of the baseline conditions. Two model parameters for uncertainty issues were changed (the hydraulic conductivity (K), porosity (n)). The parameters directly resulted in significant changes in the salt concentration distribution and the transition zone length. The amount of saline water that spread inside the aquifer for hydraulic conductivity (2K) was significantly larger than that in the case of hydraulic conductivity (K). Besides, the extent of intrusion in the low porosity case (n) was greater than that with high porosity (2n). The transition zone length was affected by each parameter change during the simulation time (Fig. 6).

4.2. Second approach

This approach depended on the initial salinity concentration distribution of the aquifer system itself bounded by the only saline source (The Mediterranean Sea) with salinity concentration of 35,000 mg/L. The initial salinity concentration distribution of the aquifer system was assigned by some polygons of different values according to the mapped salinity contour lines, which were developed based on the samples records with the help of the literature records. Then, the model was run for a long time until the natural mixing occurred between the aquifer concentration and the sea water. With this approach, the objective is to determine the precise time at which the natural mixing occurs, and perfect fitting is achieved between the calculated and observed salinity values at the various wells' locations.

The model was calibrated for both flow and salinity concentration based on values for the hydraulic conductivity of the aquifer system formation (K) and porosity (n). The nonlinearity in sensitivity parameters' calculations make the calibration process for the steady-state is complex. The root mean square error (RMSE) was calculated for salinity at the different simulation periods to define the year of simulation in which the computed and observed salinity are close (Fig. 7).

For the simulation, the 2000 year period was selected because it had a minimum RMSE of 226 mg/L, which was assumed as the steady-state condition for the model. The aquifer system is steady only when the mass concentration and flow become unchanged with simulation time. The mass balance for flow and salinity concentration translates the steady-state of the aquifer system for which the hydraulic conductivity controlled the system stability (Fig. 8). Fig. 9 illustrates the calibrated salinity concentration distribution of the aquifer.

4.2.1. Prediction scenarios

The concept that the scenarios were applied for is balancing the water demand of the development area with the available water from the existing 445 pumping wells. The development area was planned

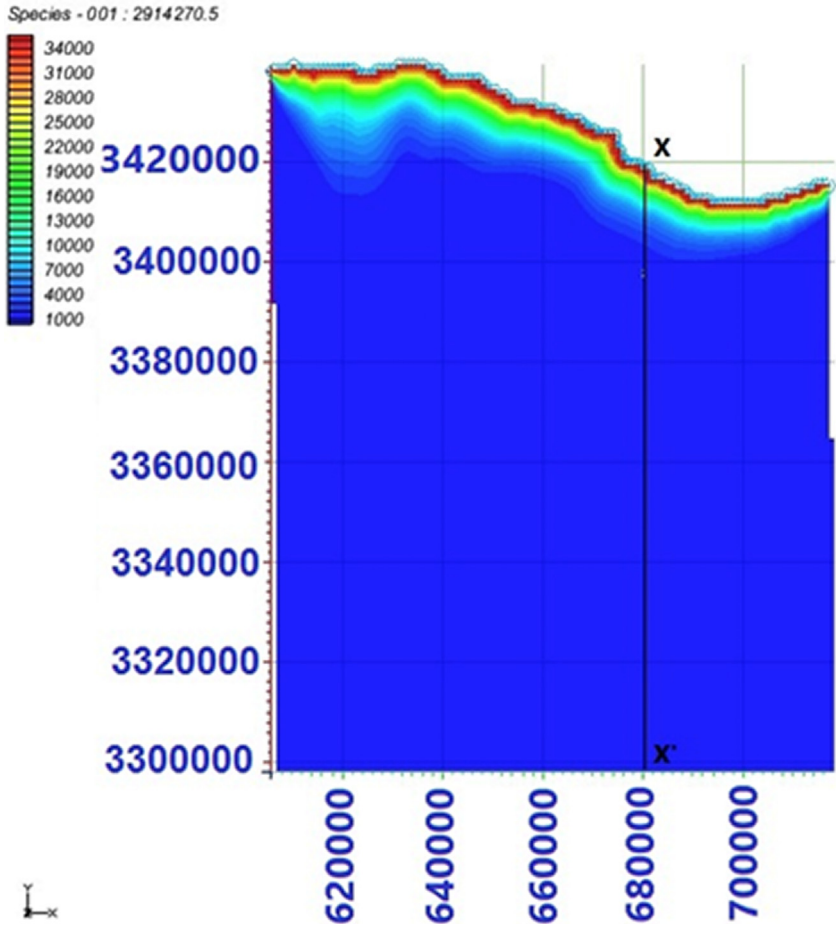

Fig. 5. (1) Salinity concentration distribution (in mg/L) in the Moghra aquifer at the last time step of the model with a simulation period of 8000 years, (2) salinity concentration distribution along the cross-section X–X′ versus time at (A) 0 years, (B) 100 years, (C) 1000 years, (D) 4000 years, and (E) 8000 years.

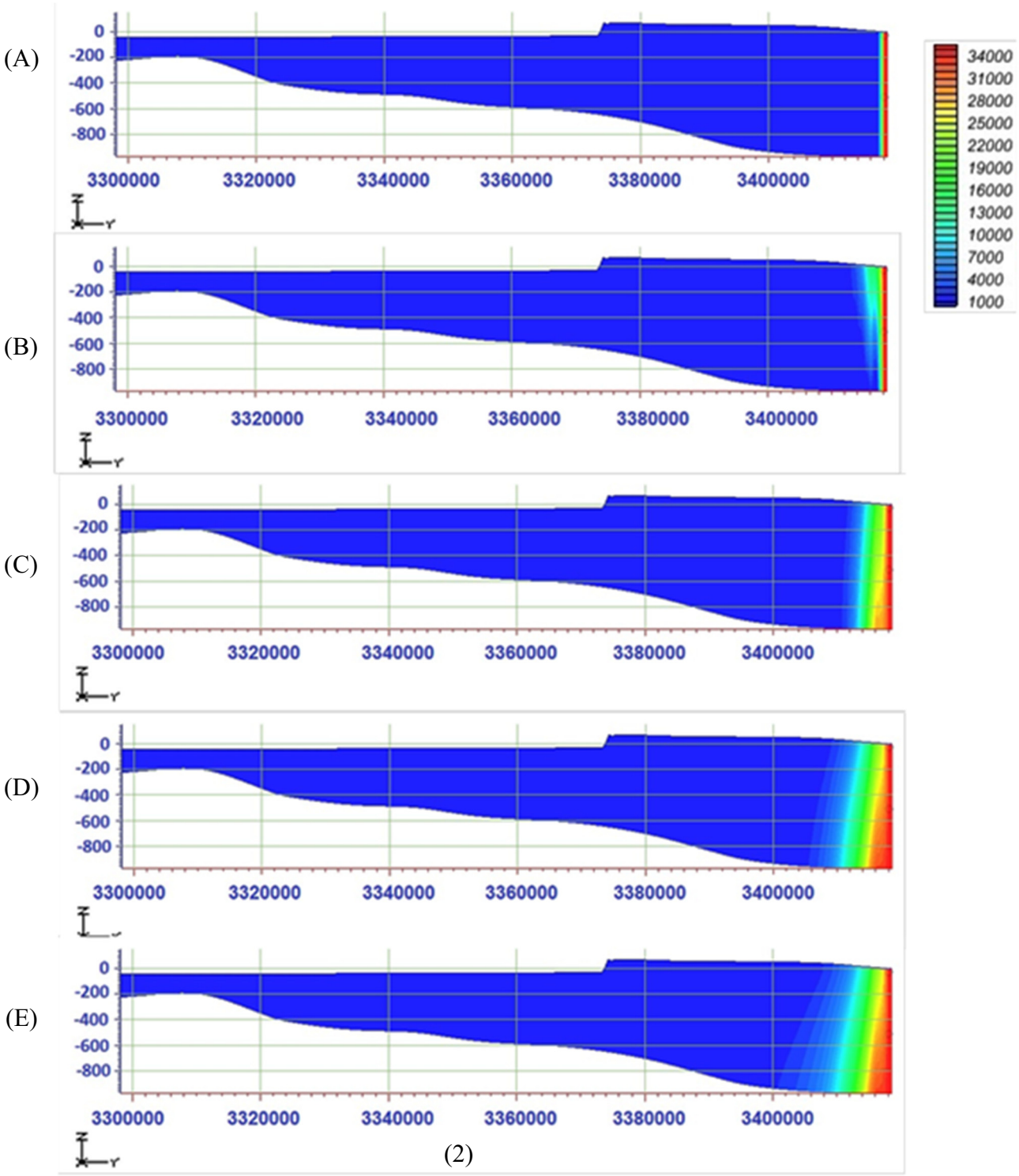

Fig. 5 (*continued*).

to serve 840 million m^2. The demand is defined according to the water duty needed for the supposed crop patterns of the development area and the area supposed to be reclaimed. Four scenarios have been applied to test the conditions of seawater intrusion caused by pumping during the next 100 years.

Scenario 1:

This represents the first stage plan for operating 465 wells, including 445 wells in the development area and 20 old wells, with the designated safe pumping rate of 1000 m^3/d. The recommended water duty for only 40% of the development area is 0.00143 $m^3/m^2/d$. The total amount of extracted water expected to be 1.63×10^{14} hm^3/y.

Scenario 2:

This scenario is same in scenario 1 but with a pumping rate of 1500 m^3/d and water duty of 0.00215 $m^3/m^2/d$. The total amount of extracted water is expected to be 2.46×10^{14} hm^3/y.

Scenario 3:

This represents well operation to meet the water requirements for the whole area in case of not drilling the second stage wells at a

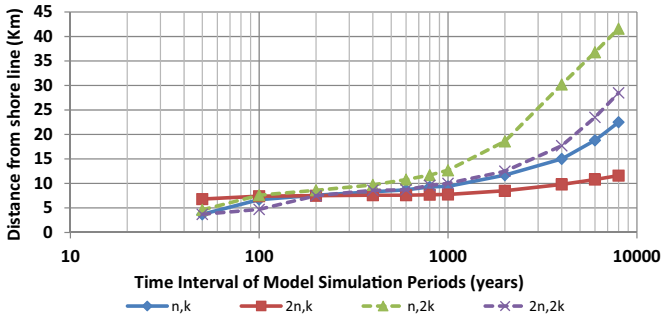

Fig. 6. Transition zone length with time (no pumping case) measured on-axis X-X′.

pumping rate of 2700 m^3/d and water duty 0.00143 m^3/m^2/d. The total amount of extracted water in this case is expected to be 4.40 × 10^{14} hm^3/y.

Scenario 4:

This is the same as Scenario 3 but with a pumping rate of 5000 m^3/d assuming that the required water duty would be raised to 0.00286 m^3/m^2/d. The total amount of extracted water is expected to be 8.21× 10^{14} hm^3/y.

A comparison of four scenarios considering the different pumping rates for 100 years is discussed below to determine the salinity changes after the well pumping operation in the development area considering different pumping rates. Some of the wells selected in the northernmost region of the bounded development area (M274, X152) in addition to two wells away from the development area domain (W8, W11) are shown to illustrate the differences in salinity and water levels by pumping (Fig. 9). Fig. 10 shows their salinity and water levels with time according to the prediction scenarios.

For scenario 1, the calculated salinity values increased with a higher rate range from 2.6% to 6.6% of the original salinity values for the wells located at the development area in the southern part of the study area (M274, X152). However, the values increased with lower rates of 0.68% to 1.16% for the two wells located in the northern part of the study area away from the development area, respectively (W8, W11). The 10,000 contour line shifted with 0.27 km from its location toward the south owing to continuous pumping. The drawdown ranged from 28.7 m to 20.6 m after 100 years for the selected wells in the development area (M274, X152) (8.2% and 5.9% of the saturated thickness, respectively). Whereas the values were 7.8 m and 2.8 m for the two wells in the northern area away from the pumping domain (W8, W11) (2.2% and 0.8% of the saturated thickness, respectively).

When operating the wells at a pumping rate of 1500 m^3/d for 100 years (Scenario 2), the salinity values increased with rates ranging from 4.08% to 9.8% of the original salinity values for the wells located in the development area in the southern part of the study area (M274, X152), respectively. However, the values increased from 1.1% to 1.8%, for the two wells located in the northern region of the study area away from the development area (W8, W11), respectively. The 10,000 contour line shifted 0.4 km from its original location owing to the continuous pumping. The drawdown ranged from 43.6 m to 31.2 m after 100 years for the wells selected in the development area (M274, X152) (12.5% and 8.9% of the saturated thickness, respectively). Whereas the values were 11 m and 4 m for the two wells in the northern part away from the pumping domain (W8, W11) (3.1% and 1.1% of the saturated thickness, respectively).

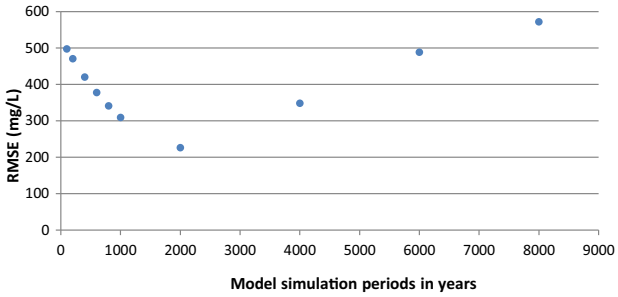

Fig. 7. RMSE of salinity values for various simulation periods.

When operating wells according to Scenario 3, the values increased with rates of 6.93% to 16.7% of the original salinity values for the wells located in the development area in the southern part of the study area (M274, X152). However, the values increased from 2.1% to 2.80% for the two wells located in the northern part of the study area away from the development area (W8, W11), respectively. The 10,000 contour line shifted 0.7 km from its original location owing to the continuous pumping. The drawdown ranged from 81 m to 58 m after 100 years for the wells selected in the development area (M274, X152) (23.1% and 16.5% of the saturated thickness), respectively. Whereas the values increased from 20 m to 7 m for the two wells in the northern part, away from the pumping domain (W8, W11) (5.7% and 2% of saturated thickness, respectively).

The fourth scenario was the critical one, with the salinity increasing at high rates of 12.6% to 26.8% of the original salinity values for the wells located at the development area in the southern part of the study area (M274, X152). However, But, the values increased to 4% for the two wells located in the northern part of the study area away from the development area (W8, W11). The 10,000 contour line shifted 0.9 km from its original location owing to continuous pumping. The drawdown ranged from 162 m to 114 m after 100 years for wells selected in the development area (M274, X152) (46.3% and 32.6% of saturated thickness, respectively), whereas, the values were 38 m and 12 m for the two wells in the northern area away from the pumping domain (W8, W11) (10.9% and 3.4% of saturated thickness, respectively).

5. Conclusion

- In this research, a 3D groundwater flow and solute transport model was set up to describe the current situation of the aquifer system flow and salinization and its behavior under different pumping conditions.
- The procedure performed for that aspect was unconventional. The first approach succeeded in defining the dividing line between the saline water and brackish water of the aquifer in the northern coastal zone for which the observation data was rare. The second approach achieved the best matching between the observed and calculated salinity values. They both gave a satisfactory result to represent the salinity delineation of the aquifer system.
- The simulation was conducted under a degree of uncertainty. So, a sensitivity analysis was set up for that aspect. It explained that the hydraulic conductivity and porosity affect the solute spread and the model simulation.
- The applied pumping scenarios yielded the following results:

a. The groundwater levels and salinity were affected by continuous pumping from the aquifer under the various rates according to the well's location. The saturated thickness was reduced to 46.3%, 10.9% under the critical pumping rate, and 8.2%, 2.2% under the designated safe pumping rate. The salinity increased by 12.6%, 4% under critical pumping rate, and 2.6%, 1.16% under the designated safe pumping rate.

b. The 10,000 contour line shifted 0.9 km from its original location under the critical pumping rate and 0.27 km under the designated safe pumping rate. The drawdown due to continuous pumping for 100 years is a little sharp and the resulted hydraulic gradient will help in saltwater intrusion into the aquifer as the water levels of

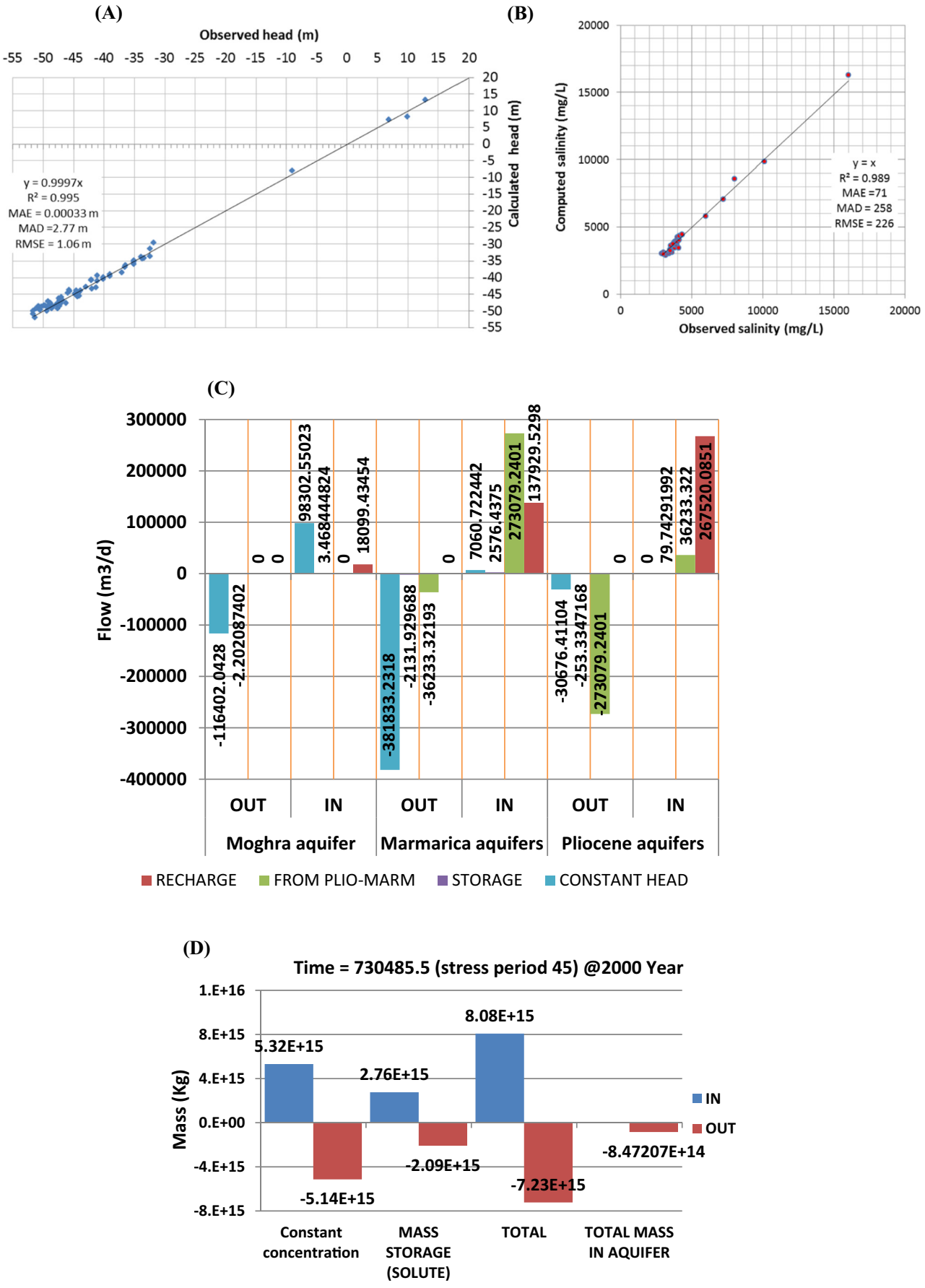

Fig. 8. (A) Computed versus observed head values for wells included in the aquifer system's calibration process, (B) computed versus observed salinity values, (C) flow budget for steady-state and (D) mass concentration balance for steady state.

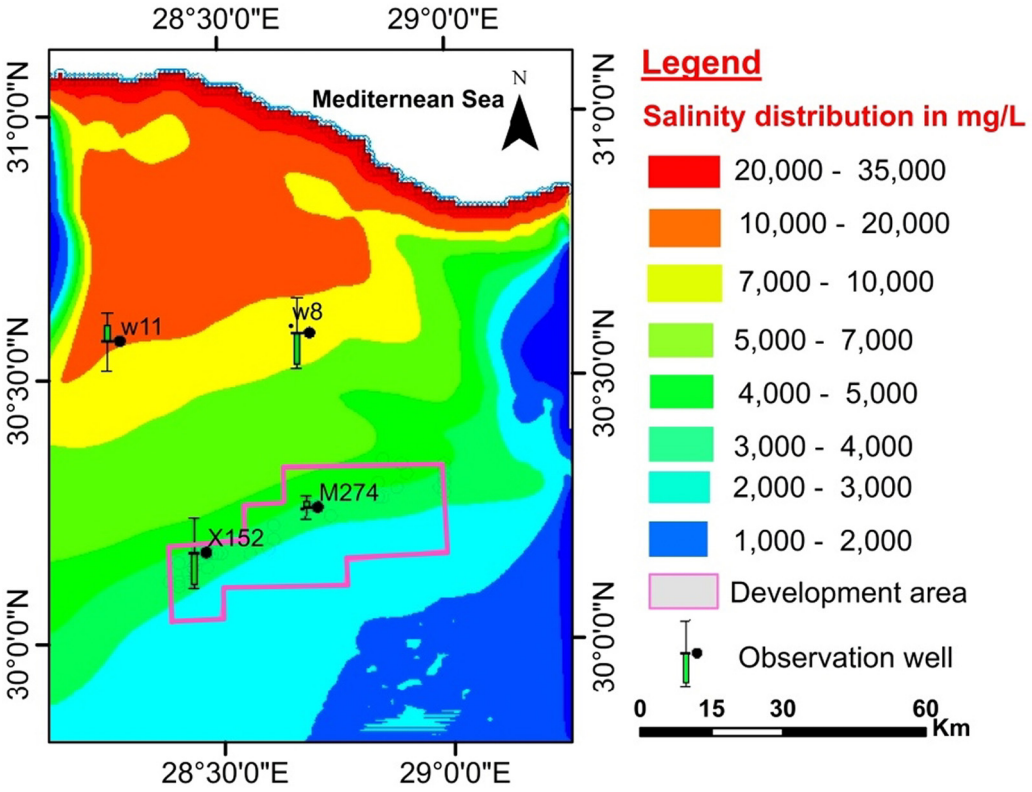

Fig. 9. Salinity concentration distribution (steady-state) and locations of observation wells.

the aquifer is below the mean seawater level.

c. Salinization of the wells by saltwater intrusion is not likely because the wells are located tens of kilometers away from the coastal zone domain. Thus, the main reason for the increase is ordinary solute transport. However, pumping affected the salinity distribution by shifting the 10,000 contour line in the northern area near the coastal

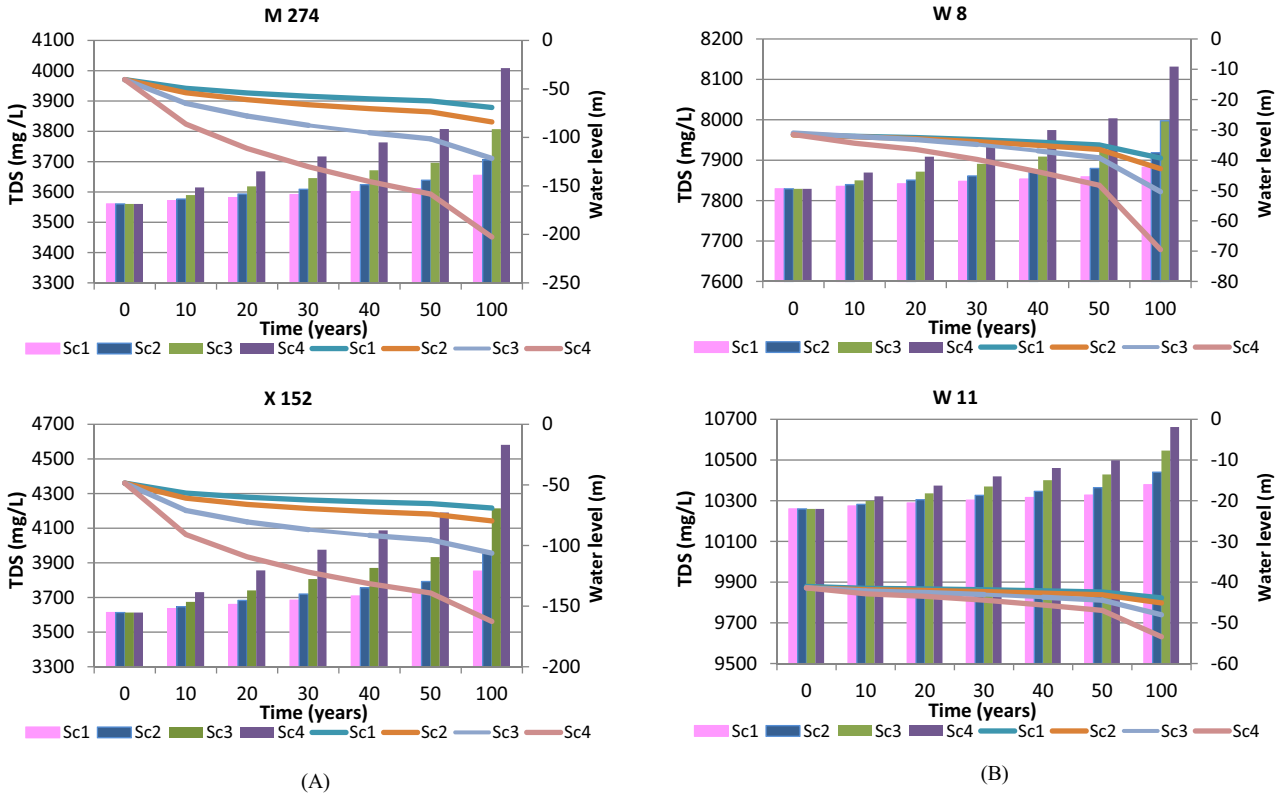

(A) (B)

Fig. 10. Salinity and water levels with time for several selected wells in (A) southern part near the development area and (B) northern part of the study area.

zone. This is directly related to the SWI issue, as mentioned during the discussion of the previous scenarios.

- The results explain that the brackishness of the aquifer is not purely attributed to the SWI. Rather, this might have been caused by the geological nature of the aquifer or old marine deposits related to the historical isotope. This can be recommended to be taken into consideration in future research plans.

CRediT authorship contribution statement

The study is part of an MSc. research conducted by S.M.G, under the supervision of E.H., T.M.H. The paper is conducted as a joint effort of all authors. Conceptualization, S.M.G, E.H., and T.M.H.; methodology, S.M.G., E.H. and T.M.H.; software, S.M.G; analysis, S.M.G; data curation, S.M.G; writing—original draft preparation, S.M.G; writing—review and editing, S.M.G., E.H, and T.M.H.; supervision, E.H, T.M.H.

Declaration of competing interest

The authors declare that they have no known competing financial interests or personal relationships that could have appeared to influence the work reported in this paper.

Acknowledgements

The activities of this research were supported by the Research Institute for Groundwater (RIGW) and the Ministry of Water Resources and Irrigation (Groundwater Sector). The authors would like to thank the review and constructive comments of the reviewers.

Funding

This research did not receive any specific grant from funding agencies in the public, commercial, or not-for-profit sectors.

Data availability statement

Research data are available from the corresponding author by request.

References

Abdallah, A.M., 1966. Stratigraphy and Structure of Apportion in the North Western Desert of Egypt, U.A.R with Reference to Its economic potentials. Geological Survey, Paper No. 45.

Abdel Mogith, S., Ibrahim, S., Hafiez, R., 2013. Groundwater potentials and characteristics of El-Moghra Aquifer in the vicinity of Qattara Depression, Egypt. J. Desert Res. 63, 1–20. doi:10.21608/ejdr.2013.5821.

Abdelhaleem, F., Helal, E., 2015. Impacts of Grand Ethiopian Renaissance Dam on different water usages in Upper Egypt. Br. J. Appl. Sci. Technol. 8, 461–483. https://doi.org/10.9734/bjast/2015/17252.

Abu-Bakr, H.A. el-A., Elkhedr, M., Hassan, T.M., 2016. Optimization of abstraction wells near coastal zone. J. Earth Sci. Res. 4, 30–42. doi:10.18005/jesr0401004

Ahmed, A.O., Khalaf, S., Abdalla, M.G., Masry, A.A. El, Author, C., Ahmed, A.O., 2015. Groundwater Management in Wadi El Natrun Pliocene Aquifer, Egypt. 6 pp. 291–302.

Allam, A., Helal, E., Mansour, M., 2019. Retarding contaminant migration through porous media using inclined barrier walls. J. Hydrol. Hydromechanics 67, 339–348. https://doi.org/10.2478/johh-2019-0020.

Badaruddin, S., Morgan, L.K., 2017. Characteristics of active seawater intrusion. J. Hydrol. 551, 632–647. https://doi.org/10.1016/J.JHYDROL.2017.04.031.

Badaruddin, S., Werner, A.D., Morgan, L.K., 2017. Characteristics of active seawater intrusion. J. Hydrol. 551, 632–647. https://doi.org/10.1016/j.jhydrol.2017.04.031.

Chang, Y., Hu, B.X., Xu, Z., Li, X., Tong, J., Chen, L., Zhang, H., Miao, J., Liu, H., Ma, Z., 2018. Numerical simulation of seawater intrusion to coastal aquifers and brine water/freshwater interaction in south coast of Laizhou Bay, China. J. Contam. Hydrol. 215, 1–10. https://doi.org/10.1016/j.jconhyd.2018.06.002.

Davis & De Wiest (1967): Hydrogeology: JohnWiley & Sons, Inc. New York, 463p.

Ezzat, D.M.A., 1984. Qattara Hydro Energy Project Side Effects on Groundwater Aquifers.

Farooq, S.H., 2020. Seawater intrusion in the coastal aquifers of India - a review. HydroResearch 3, 61–74. https://doi.org/10.1016/j.hydres.2020.06.001.

Guo, W., Bennett, G.D., 1998. Simulation of saline/fresh water flows using MODFLOW. Proc. MODFLOW'98 Conf., Oct. 4–8, 1998, Golden, Color. USA 267–274.

Gumus, V., Simsek, O., Soydan, N.G., Akoz, M.S., Kirkgoz, M.S., 2016. Numerical modeling of submerged hydraulic jump from a sluice gate. J. Irrig. Drain. Eng. 142 (1). https://doi.org/10.1061/(ASCE)IR.1943-4774.0000948 04015037.

Guo, W., Langevin, C.D., 2002. User's Guide to SEAWAT: A Computer Program for Simulation of Three-dimensional Variable-density Ground-water Flow USGS Techniques of Water Resources Investigations.

Kazakis, N., Spiliotis, M., Voudouris, K., Pliakas, F.K., Papadopoulos, B., 2018. A fuzzy multicriteria categorization of the GALDIT method to assess seawater intrusion vulnerability of coastal aquifers. Sci. Total Environ. 621, 524–534. https://doi.org/10.1016/j.scitotenv.2017.11.235.

Korany, 1975. Geological and Hydrogeological Studies of the Area Between Burg Al Arab and El Dabaa, North Western Desert of Egypt. PhD., Thesis Ain Shams University, Faculty of Science.

Langevin, C.D., Hughes, J.D., Panday, S., Provost, A., Niswonger, R., 2016. Past, Present, and Future Directions for Saltwater Intrusion Modeling Using SEAWAT 20192.

Mabrouk, M., Jonoski, A., Essink, G.H.P.O., Uhlenbrook, S., 2019. Assessing the fresh-saline groundwater distribution in the Nile delta aquifer using a 3D variable-density groundwater flow model. Water (Switzerland) 11. https://doi.org/10.3390/w11091946.

Mansour, M.M., Ellayn, A.F., Helal, E., Rashwan, I.M.H., Sobieh, M.F., 2018. Delaying solute transport through the soil using unequal double sheet piles with a surface floor. Ain Shams Eng. J. 9, 3399–3409. https://doi.org/10.1016/j.asej.2018.10.003.

Morad, N.A., Masoud, M.H., Abdel Moghith, S.M., 2014. Hydrologic factors controlling groundwater salinity in northwestern coastal zone. Egypt. J. Earth Syst. Sci. 123, 1567–1578. https://doi.org/10.1007/s12040-014-0483-3.

Negm, A.M., 2019. Groundwater in the Nile Delta.

Nofal, E.R., Amer, M.A., El-Didy, S.M., Fekry, A.M., 2015. Delineation and modeling of seawater intrusion into the Nile Delta Aquifer: a new perspective. Water Sci. 29, 156–166. https://doi.org/10.1016/j.wsj.2015.11.003.

Oude Essink, G.H.P., Boekelman, R.H., 1998. Problems with large-scale 3D modeling of salt water intrusion. Boletín Geológico y Min. 109, 87–104.

Polemio, M., Zuffianò, L.E., 2013. Overview of Groundwater Management Approaches at Salinisation Risk. 15 p. 4591.

Pool, M., Post, V.E.A., Simmons, C.T., 2014. Effects of Tidal Fluctuations on Mixing and Spreading in Coastalaquifers: Homogeneous Case 6910–6926. https://doi.org/10.1002/2014WR015534.Received.

Pool, M., Post, V.E.A., Simmons, C.T., 2015. Effects of Tidal Fluctuations and Spatial Heterogeneity Onmixing and Spreading in Spatially Heterogeneous Coastalaquifers 1570–1585. https://doi.org/10.1002/2014WR016068.Received.

RIGW, 2006. Hydro-geological Map of Alexandria. Scale 1:100000. (first edition).

RIGW, 2018. Explanatory Technical Note for the Hydrological Map of El Mogha Area No. (9), Scale 1:100000 Related to Digitizing and Updating the Hydrological Statements for Some Development Areas' Project with the Help of Academy of Scientific Research & Technology.

Roache, P.J., 1998. Verification of codes and calculations. AIAA J. 36 (5), 696–702. https://doi.org/10.2514/2.457.

Sakr, S.A., 1992. Vertically Integrated Two Dimensional Finite Element Model of Sea Water Intrusion in Aquifers.

Sakr, S.A., Attia, F.A., Millette, J.A., 2004. Vulnerability of the Nile Delta aquifer of Egypt to seawater intrusion. International Conference on Water Resources of arid and Semi-arid Regions 25 of Africa, Issues and Challenges, Gaborone, Botswana.

Sarker, M.R., Camp, M. Van, Islam, M., Ahmed, N., 2018. Salinity Distribution in Different Coastal Aquifers of Southwest 2018.

Sayed, M.M.A.E.G., 2018. Assessment of Groundwater Resources in the Area East of Qattara Depression, North Western Desert, Egypt - Using Hydrogeological and Isotope Techniques/173.

Sefelnasr, A., Sherif, M., 2014. Impacts of Seawater Rise on Seawater Intrusion in the Nile Delta Aquifer, Egypt. 52, pp. 264–276. https://doi.org/10.1111/gwat.12058.

Sherif, M., Sefelnasr, A., Ebraheem, A.A., Javadi, A., 2014. Quantitative and qualitative assessment of seawater intrusion in Wadi Ham under different pumping scenarios. J. Hydrol. Eng. https://doi.org/10.1061/(ASCE)HE.1943-5584.0000907.

Sobeih, M.M., El-Arabi, N.E., Helal, E.E.D.Y., Awad, B.S., 2017. Management of water resources to control groundwater levels in the southern area of the western Nile delta. Egypt. Water Sci. 31, 137–150. https://doi.org/10.1016/j.wsj.2017.09.001.

Stein, S., Kasher, R., Yechieli, Y., Sivan, O., n.d. Modeling the Impact of Saline Groundwater Pumping From Coastal Aquifers Beneath the Fresh-saline Water Interface for Desalination Purposes 282.

Verkaik, J., Huizer, S., Van Engelen, J., Ram, R., Vuik, K., Oude Essink, G.H.P., 2018. Parallel Computing With SEAWAT. 25nd Salt Water Intrusion Meet. 347.

Yousif, M., Bubenzer, O., 2012. Perched groundwater at the northwestern coast of Egypt: a case study of the Fuka Basin. Appl Water Sci 2, 15–28. https://doi.org/10.1007/s13201-011-0023-0.

Yousif, M., Bubenzer, O., 2013. An integrated approach for groundwater assessment at the Northwestern Coast of Egypt (Ras El Hekma area): case study. Environ. Earth Sci. 69, 2227–2246. https://doi.org/10.1007/s12665-012-2052-x.